Quantum Electronics **34** (4) 348 – 354 (2004)

NONLINEAR OPTICAL PHENOMENA

PACS numbers: 42.65.Re; 42.65.An; 42.65.Jx
DOI: 10.1070/QE2004v034n04ABEH002679

Supercontinuum sources in a high-power femtosecond laser pulse propagating in liquids and gases

V.P. Kandidov, I.S. Golubtsov, O.G. Kosareva

***Abstract*. The mechanism of supercontinuum generation and the spatial distribution of its sources during the propagation of a high-power femtosecond laser pulse in liquids and gases are studied. The numerical simulation shows that the supercontinuum is generated due to self-phase modulation of the laser pulse in space and time in the presence of nonlinearity and wave effects. Supercontinuum sources are found to be located mainly in the ring structure of the laser pulse at the intensity minima. It is established that the efficiency of generation of the short-wavelength part of the supercontinuum during the propagation of the focused laser beam depends on the initial phase modulation and achieves a maximum when the compression length slightly exceeds the length of nonlinear focusing.**

Keywords: *filamentation, supercontinuum sources, phase modulation.*

1. Introduction

The spatial and temporal characteristics of high-power femtosecond pulses strongly change during their propagation in transparent dielectrics due to the nonlinear interaction of the laser field with the medium. One of manifestations of these changes is a very strong broadening of the frequency spectrum of the pulse – the formation of a supercontinuum at high energy densities of the light field [1, 2]. The spatial density of energy in dielectrics is achieved due to nonlinear and geometrical focusing of radiation [3 – 5], while the density of energy in time is produced upon nonlinear compression of laser pulses [6, 7].

The results of many experiments with laser pulses propagating in condensed media and gases demonstrate the similarity of supercontinuum spectra [4, 8, 9]. A laser pulse broadens during its interaction with a medium up to a few hundreds of nanometres, both to the Stokes and anti-Stokes regions. The broadening to the blue usually dominates. The frequency spectrum of the supercontinuum is continuous and does not contain distinct spectral lines. The anti-Stokes wing of the supercontinuum has, as a rule, a nontrivial angular distribution representing conical emission with the divergence angle increasing with decreasing wavelength [4, 5, 10].

The nature of supercontinuum and conical emission, as a part of the continuum, has been interpreted differently. In the first papers [1, 11] devoted to this subject, the generation of the supercontinuum was explained by the temporal self-phase modulation of the light field. At the same time, the numerical estimates of the broadening of the spectrum performed using the model of plane waves proved to be substantially lower than the experimental broadening. The appearance of conical emission was explained by the Čerenkov effect [12] and by four-wave parametric interaction in the case of the Kerr nonlinearity [10]. However, according to the last hypothesis, conical emission should be observed in the Stokes region of the spectrum as well, which was not found in experiments.

It was assumed in Ref. [3], where the supercontinuum was observed for the first time in gases, that an extremely strong broadening of the laser-pulse spectrum can be explained by taking into account not only a nonlinear transformation of the pulse in time but also its spatial variations caused by the effect of self-focusing and a laser plasma. Many authors discussed the nature of conical emission pointing to an inseparable relation between the spatial and temporal modulations. It was shown in review [13] that in the case of the resonance interaction of laser radiation with a two-level atomic medium, the spatiotemporal modulation of the laser pulse produces sideband harmonics in the spectrum propagating at an angle to the axis. The author of Ref. [14] considered theoretically the generation of the supercontinuum upon focusing a laser beam to argon at high pressures and concluded that the time gradient of the refractive index of the medium can take place only in the presence of the corresponding spatial gradient, and therefore the spectral components of the pulse acquire the angular divergence along with the frequency shift. The authors of Ref. [15] studied experimentally and theoretically the propagation of a picosecond laser pulse in a quasi-resonance medium – cesium and barium vapours and explained the angular divergence by the spatial self-phase modulation of the light field in the beam cross section. The

V.P. Kandidov Department of Physics, M.V. Lomonosov Moscow State University, Vorob'evy gory, 119992 Moscow, Russia; tel.: 939-30-91; web-site: http://www.phys.msu.su;
I.S. Golubtsov, O.G. Kosareva International Teaching and Research Laser Center, M.V. Lomonosov Moscow State University, Vorob'evy gory, 119992 Moscow, Russia; tel.: 939-30-91; web-site: http://www.msuilc.phys.msu.su

Received 11 December 2003
Kvantovaya Elektronika **34** (4) 348 – 354 (2004)
Translated by M.N. Sapozhnikov

spectral maps of the supercontinuum observed upon a tight focusing of laser beams to various gases were obtained experimentally [16] and theoretically [14].

The physical model of the supercontinuum generation during the propagation of a high-power femtosecond laser pulse due to the self-phase modulation of radiation in space and time was developed consistently in Refs [2, 4, 17–19]. According to this model, a nonlinear phase shift, appearing due to the interaction of the laser pulse with the medium in the case of a high spatiotemporal localisation of energy, has substantial time and spatial gradients, which lead to the broadening of the frequency spectrum and the appearance of the angular divergence. A combined contribution from the inseparable Kerr and plasma nonlinearities, wave diffraction effects and the material dispersion of air causes an extreme broadening of the frequency-angular spectrum of the laser pulse, which is observed as the supercontinuum and conical emission. The role of the wave instability, which leads to an increase in the steepness of the trailing edge of the femtosecond pulse during its self-focusing in a nonlinear medium, resulting in the broadening of the blue wing of the pulse spectrum, was analysed in Refs [2, 20].

The aim of this paper is to study in detail the supercontinuum generation during the propagation of high-power femtosecond laser pulses in continuous transparent media and to find the location of sources of spectral components and to determine their nature.

2. Model of the nonlinear-optical interaction

The supercontinuum generation during the propagation of high-power femtosecond laser pulses in continuous transparent media is described by the model considered in detail in Refs [18, 19]. This model uses the slowly varying envelope approximation, which adequately describes [21–23] the transformation of pulses of duration as short as a few optical cycles. The equation for the amplitude of the light field E of a femtosecond laser pulse has the form [2]

$$2ik\frac{\partial E}{\partial z}=\left(1-\frac{i}{\omega_0}\frac{\partial}{\partial\tau}\right)^{-1}\Delta_\perp E-kk_\omega''\frac{\partial^2 E}{\partial\tau^2}+\frac{i}{3}kk_\omega'''\frac{\partial^3 E}{\partial\tau^3}$$

$$+\frac{2k^2}{n_0}\left[\left(1-\frac{i}{\omega_0}\frac{\partial}{\partial\tau}\right)\Delta n_k+\left(1+\frac{i}{\omega_0}\frac{\partial}{\partial\tau}\right)\Delta n_p\right]E-ik\alpha E. \quad (1)$$

Here, k is the wave-vector modulus; k_ω'' and k_ω''' are its derivatives with respect to the carrier frequency; n_0 is the refractive index of the medium; α is the absorption coefficient related to the photoionisation losses of radiation; and $\Delta_\perp=\partial^2/\partial r^2+r^{-1}\partial/\partial r$.

The first term in the right-hand side of (1) describes the beam diffraction, the second and third ones describe the material dispersion in the third approximation of the dispersion theory, the fourth term describes contributions from the Kerr (Δn_k) and plasma (Δn_p) nonlinearities to the refractive index of the medium, and, finally, the last term describes photoionisation energy losses. Operators of the type $\pm(i/\omega_0)(\partial/\partial\tau)$, where ω_0 is the laser frequency, describe the effect of the wave instability, which results, in particular, in an increase in the steepness of the trailing edge of the pulse in the Kerr medium.

The change in the refractive index caused by the Kerr nonlinearity, taking into account the nonstationary contribution of stimulated Raman scattering from vibrational molecular transitions of the medium, has the form

$$\Delta n_k=\frac{1}{2}n_2|E|^2+\frac{1}{2}\int_{-\infty}^{t}\frac{1}{2}n_2|E(r,t')|^2H(t-t')dt', \quad (2)$$

where $H(t)$ is the transfer function presented in Ref. [24].

The nonlinearity of the laser plasma produced upon multiphoton collision ionisation in the intense laser field is described by the expression

$$\Delta n_p=-\frac{\omega_p^2}{2n_0(\omega_0^2+\nu_c^2)}\left(1-i\frac{\nu_c}{\omega_0}\right), \quad (3)$$

where $\omega_p=(4\pi e^2N_e/m)^{1/2}$ is the plasma frequency; N_e is the density of free electrons; and $\nu_c=N_0v_e\sigma_c$ is the effective frequency of collisions between electrons and molecules of the medium. The change in the density N_e of free electrons is described by the rate equations

$$\frac{\partial N_e}{\partial t}=R(|E|^2)(N_0-N_e)+\nu_iN_e-\beta N_e^2, \quad (4)$$

where ν_i is the frequency of ion–electron collisions; R is the ionisation rate of the medium; and β is the radiative recombination coefficient.

The spatial and temporal variation of the electric field is described in this paper by a Gaussian, which is close to experimental data [8]:

$$E(r,z=0,\tau)=E_0\left(\frac{\tau_0}{\tau_p(\delta)}\right)^{1/2}$$

$$\times\exp\left(-\frac{r^2}{2a_0^2}-\frac{\tau^2}{2\tau_p^2(\delta)}+i\frac{kr^2}{2R_f}+i\frac{\delta\tau^2}{2}\right), \quad (5)$$

where a_0 is the beam radius and R_f is the geometrical focusing length (distance from a lens to the beam waist). The initial pulse duration $\tau_p(\delta)$ and the parameter δ, which characterises the value of the phase modulation of the pulse with a constant width $\Delta\omega_{e^{-1}}$ of the frequency spectrum at the e^{-1} level are related by the expression [7]

$$\delta=\pm\frac{[(\tau_p(\delta)/\tau_0)^2-1]^{1/2}}{\tau_p^2(\delta)}, \quad (6)$$

where $\tau_0=(\Delta\omega_{e^{-1}})^{-1}=\tau_p(\delta=0)$ is the transform-limited pulse duration; the plus and minus signs in the right-hand side correspond to the positive and negative phase modulation, respectively.

3. Supercontinuum sources and transformation of a laser pulse

The nonlinear-optical transformation of a laser pulse is manifested in the change in the spatiotemporal dependences of the pulse envelope $E(r,t,z)$ and its frequency-angular spectrum $E(\omega,\theta,z)$ with z. A two-way analysis of the light field of the laser pulse allows one to explain the physical nature of the supercontinuum generation and to study the process of formation of its sources.

Let us analyse, for example, a femtosecond laser pulse focused to a cell with water. Such experiments were performed in Ref. [8] with 0.2–3 μJ, 800-nm pulses from a Ti : sapphire laser. The FWHM duration of pulses was

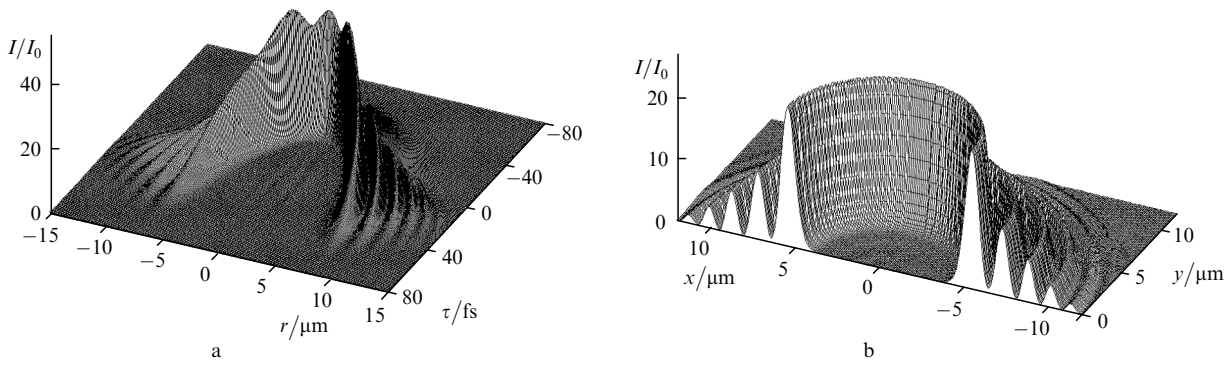

Figure 1. Spatiotemporal intensity distribution $I(r,\tau)$ in the (r,τ) plane (a) and the radial intensity distribution $I(x,y)$ for $\tau = 0$ (b) for the laser pulse in a cell with water located at a distance of 40 μm from the geometrical focus (in front of it) of the cell with $R_f = 16.9$ mm. The pulse duration is $\tau_{0.5} = 45$ fs and its energy is $W_0 = 3$ μJ. The pulse intensity is normalised to $I_0 = 10^{12}$ W cm^{-2}.

45 fs and the laser beam diameter was 5 mm. The beam focusing length R_f was varied from 10 to 74 mm. A supercontinuum pulse propagating forward was recorded whose energy increased with increasing the laser pulse energy and the focal distance of the objective.

This experiment was simulated numerically by solving the system of equations (1)–(4) by the method of splitting over physical factors using the sweep method for integration with respect to the radial coordinate r, the spectral representation for integration with respect to time t, and an adaptive step over the evolution coordinate z. The computational grid had 2048×2048 nodes over coordinates r and t. The number of steps along the z axis was varied from 3600 (fo $R_f = 73.5$ mm) to 5800 (for $R_f = 16.9$ mm).

Because of the geometrical and Kerr focusing, the intensity at the pulse axis increases up to the value $\sim 4 \times 10^{13}$ W cm^{-2}, at which multiphoton and avalanche ionisation develop in water. Defocusing in the produced laser plasma restricts a further increase in the pulse intensity. The nonlinear refraction of the trailing edge of the pulse caused by the Kerr and plasma nonlinearities leads to the formation of a complex ring structure in the pulse cross section. Figure 1 shows the spatiotemporal distribution of the intensity $I(r,\tau)$ and the radial distribution of the intensity $I(x,y)$ at the central layer of the pulse ($\tau = 0$) in a cell with water at a distance of 40 μm from the geometrical focus (in front of it) of a lens with $R_f =$ 16.9 mm.

Figure 1b gives a complete picture of the spatiotemporal intensity distribution in the pulse at this distance. In this case, the pulse intensity takes its maximum in the temporal layer for $\tau = -40$ fs. The next layers of the pulse decompose into concentric rings whose radius increases toward the pulse tail.

The formation of the intensity rings in the cross section of temporal layers of the pulse is accompanied by the appearance of a continuous high-frequency wing in the frequency-angular spectrum, whose components propagate at an angle to the optical axis. This radiation represents conical emission in which the divergence of the frequency components increases with decreasing wavelength. The intensity distribution of conical emission is illustrated in Fig. 2, where the lines $S(\lambda,\theta) = \text{const}$ of equal spectral power density of the frequency-angular spectrum of the laser pulse are plotted in the wavelength-radiation divergence angle plane (λ,θ). Conical emission extends to the high-frequency region down to 400 nm, whereas it is absent in the low-frequency region. For the chosen level of the spectral power density (for example, $\lg S(\lambda,\theta)/S_{max} = -1$, -2, etc.), the radiation divergence angle θ of the anti-Stokes components ($\lambda < 800$ nm) increases with decreasing their wavelength λ, whereas θ is close to zero for Stokes components ($\lambda > 800$ nm).

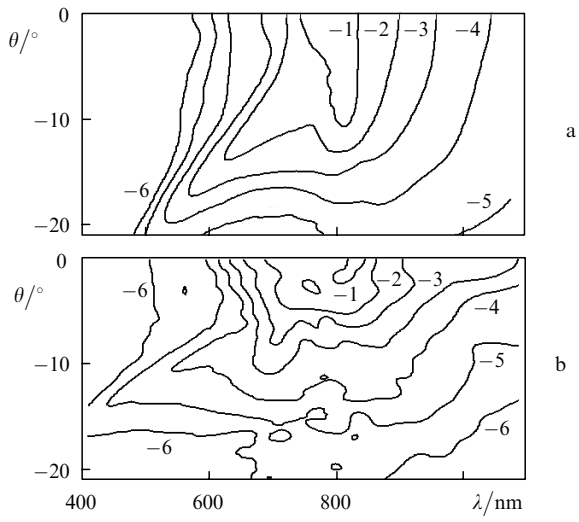

Figure 2. Frequency-angular spectrum represented by the lines $S(\lambda,\theta)$ of equal power density of spectral components of the laser pulse with $\tau_{0.5} = 45$ fs and $W_0 = 3$ μJ focused into a cell with water for $R_f = 16.9$ mm (the observation plane is located at the distance $z = 40$ μm from the geometrical focus of the lens) (a) and $R_f = 43.1$ mm ($z = 120$ μm from the geometrical focus of the lens) (b). The power density levels are presented at the logarithmic scale normalised to the maximum ($\lg S(\lambda,\theta)/S_{max} = -1$, -2, etc.).

One can see from Fig. 2 that the divergence angle of conical emission increases with decreasing R_f. To explain this, we will assume that the angle α_{con} of conical emission from a focused beam is equal to the sum of the divergence angle α_{dif} of the pump beam in the absence of nonlinearity and the angle α_{col} of conical emission from a collimated beam:

$$\alpha_{con} = \alpha_{dif} + \alpha_{col}, \quad (7)$$

where $\alpha_{dif} = \pi n_0 a_0/(2R_f)$. For $R_f = 16.9$ mm, the angle $\alpha_{dif} = 13^\circ$, and for $R_f = 43.1$ mm, $\alpha_{dif} = 5^\circ$. According to Fig. 2, the angle α_{con} of conical emission at a wavelength of 500 nm for these focal distances is 21° and 12°, respectively. The angles of conical emission α_{col} estimated from (7) for these two focal distances are close. Therefore, the assumption about the additivity of contributions from the divergence of the pump beam and conical emission to the resulting divergence of the short-wavelengths components of the supercontinuum in a focused beam is valid.

The radial distribution of the spectral power of the supercontinuum components in the region of the geometrical focus of the lens for $R_f = 16.9$ mm is shown in Fig. 3 as a map in the radius-wavelength plane (r, λ). Darker regions correspond to the higher power density of the corresponding spectral components. One can see that the energy of the long-wavelength ($\lambda > 800$ nm) components of the supercontinuum is mainly localised on the pulse axis, whereas the energy of the short-wavelength ($\lambda < 800$ nm) components is localised at its periphery in the ring structure of a filament (see Fig. 1).

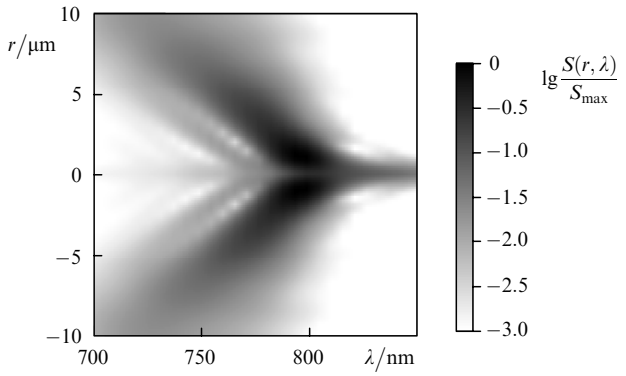

Figure 3. Radial distribution of the spectral power density $S(r, \lambda)$ of the laser pulse in a cell with water in the region of the geometrical focus of the lens for $\tau_{0.5} = 45$ fs, $W_0 = 3$ μJ, and $R_f = 16.9$ mm. The darker regions correspond to a greater power density S/S_{max} of spectral components.

The assumption that the supercontinuum is produced due to the self-phase modulation of a laser pulse upon the nonlinear phase shift in space and time allows us to determine the localisation of sources of the spectral components. The self-phase modulation of the light field of the laser pulse leads to the radiation frequency shift and the angular divergence of spectral components. The frequency shift of the supercontinuum harmonics with respect to the carrier frequency is determined by the phase gradient in time: $\Delta\omega(r, \tau) = \partial\varphi(r, \tau)/\partial\tau$, and the angle θ at which radiation propagates is determined by the spatial gradient: $\theta(r, \tau) = \arctan[-(1/k)(\partial\varphi(r, \tau)/\partial r)]$. Figure 4 shows the spatial localisation of sources of the spectral components of supercontinuum and their angular directivity. Here, we present the radial distributions $I(r, \tau = 0)$ of the laser pulse intensity, the wavelength of the supercontinuum sources determined by the relation $\lambda(r, \tau = 0) = 2\pi c/[\omega_0 + \Delta\omega(r, \tau = 0)]$, and of the radiation divergence angle $\theta(r, \tau = 0)$ for the temporal layer $\tau = 0$ of a pulse focused by a lens with $R_f = 16.9$ mm into a cell with water.

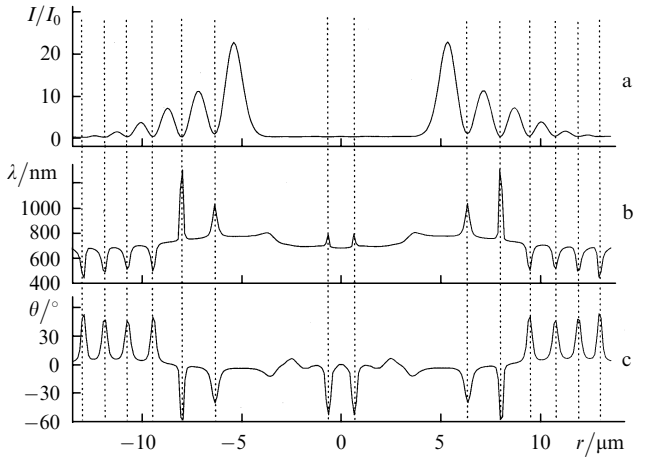

Figure 4. Radial distributions of the laser pulse intensity $I(r, \tau = 0)$ (a), the wavelength $\lambda(r, \tau = 0) = 2\pi c/[\omega_0 + \delta\omega(r, \tau = 0)]$ of supercontinuum sources (b), and the divergence angle $\theta(r, \tau = 0)$ of their radiation (c) in the temporal layer $\tau = 0$ of the laser pulse in a cell with water located at a distance of 40 μm from the geometrical focus (in front of it) of the lens for $\tau_0 = 45$ fs, $W_0 = 3$ μJ, and $R_f = 16.9$ mm. The negative and positive values of the angle θ correspond to the convergence and divergence of radiation to the optical axis, respectively. The pulse intensity is normalised to $I_0 = 10^{12}$ W cm^{-2}.

One can see that the supercontinuum sources are predominantly located in the ring structure of the laser pulse, not only near the optical axis but also at the beam periphery. The frequency shift is maximal at the minima of the intensity of the ring structure, which appeared due to the interference of energy fluxes in the beam cross section. One of the fluxes propagates towards the optical axis under the action of self-focusing and geometrical focusing, whereas the second flux propagates in the opposite direction due to radiation defocusing in the laser plasma. The interference of waves during the propagation of the laser pulse leads to the formation of edge phase dislocations [25], where the supercontinuum generation occurs. The pulse phase in the dislocation vicinity strongly changes in space and time, resulting in the generation of new frequency components and the angular divergence. Therefore, conical emission is generated namely in the region of phase dislocations of the ring structure of the laser pulse.

By comparing the radial dependences of the wavelength $\lambda(r)$ and the divergence angle $\theta(r)$ of radiation from supercontinuum sources of the laser pulse, we can see that the sources of low-frequency components are located close to the intensity rings $I(r)$ nearest to the optical axis and their radiation is directed to the axis. The sources of high-frequency components with $\lambda < 600$ nm are localised near the periphery rings $I(r)$ and their radiation is directed from the axis. As a result, the short-wavelength radiation has the angular divergence, whereas the low-frequency harmonics propagate predominantly along the optical axis, which is confirmed experimentally [4, 21].

4. Effect of the wave instability on the supercontinuum generation

The self-phase modulation of the light field resulting in the supercontinuum generation is caused by various nonlinear-optical mechanisms of the interaction of high-power laser radiation with a medium. Thus, the nonlinear phase shift in

the axial region at the leading edge of the pulse is mainly determined by the Kerr nonlinearity of the medium because an increase in the density of free electrons is still not sufficient. A drastic increase in the pulse intensity with time $[\partial I(r,\tau)/\partial\tau > 0]$ due to this nonlinearity leads to a negative shift of the radiation frequency: $\Delta\omega(r,\tau) \sim -\partial I(r,\tau)/\partial\tau < 0$. A drastic decrease in the intensity at the trailing edge of the pulse $[\partial I(r,\tau)/\partial\tau < 0]$ upon pulse defocusing in the laser plasma leads to a positive shift of the radiation frequency.

The supercontinuum generation during the propagation of femtosecond laser pulses is substantially determined by the wave instability described by operators $\pm(\mathrm{i}/\omega_0)(\partial/\partial\tau)$ in Eqn (1). The wave instability leads to an increase in the steepness of the trailing edge of the pulse and a decrease in the steepness of the leading edge, resulting in the broadening of the spectrum in the short-wavelength region and narrowing of the spectrum in the long-wavelength region [19, 20].

The effect of the steepness of the trailing edge of the pulse on the supercontinuum generation is demonstrated in Fig. 5 where the spatiotemporal intensity distributions and frequency-angular spectra of the laser pulse in the air are presented. These results were obtained by solving the system of equations (1)–(4) for the 230-fs, 8-mJ laser pulse and the laser beam diameter of 0.28 mm [17]. At the distance $z = 0.43L_{\mathrm{dif}}$ (L_{dif} is the diffraction length), the trailing edge of the laser pulse acquires a ring structure under the action of the Kerr and plasma nonlinearities (Fig. 5a), which is manifested in the spectral space as conical emission in the anti-Stokes region (Fig. 5b). Upon a further propagation ($z = 0.6L_{\mathrm{dif}}$), the laser pulse is decomposed into a pair of pulses (Fig. 5c), the steepness of the trailing edge of the second pulse giving rise to the broadening of the spectrum in the anti-Stokes region (Fig. 5d).

We analysed the influence of self-steepening by calculating the spatiotemporal intensity distribution and frequency-angular spectrum of the laser pulse in the air at the distance $z = 0.6L_{\mathrm{dif}}$ in the absence of operators $\pm(\mathrm{i}/\omega_0)(\partial/\partial\tau)$. A comparison of Figs 5c and e and Figs 5d and f shows that the trailing edge of the second pulse has a larger gradient due to self-steepening; this is manifested in the frequency-angular spectrum in a stronger broadening of the laser pulse spectrum in the anti-Stokes region.

5. Supercontinuum generation in a focused beam in the presence of the initial phase modulation of the pulse

The possibility of increasing the energy density in the interaction region upon compression of pulses with the initial negative phase modulation in media with a normal dispersion was studied in Refs [6, 7]. It was shown that the efficiency of supercontinuum generation by collimated high-power femtosecond laser pulses achieved a maximum when the compression length L_{com} was close to the self-focusing length L_{sf}. To verify the correctness of this conclusion for focused radiation, we consider the propagation in the air of a pulse with the initial phase modulation and $W_0 = 60$ mJ, the diameter of the initial beam $2a_0 = 6$ cm, and $R_{\mathrm{f}} = 0.3L_{\mathrm{dif}}$. The FWHM pulse duration in the absence of phase modulation is $\tau_{0.5} = 35$ fs.

Figure 6 shows the maximum intensity of the laser pulse and the energy of the supercontinuum blue wing as functions of the distance z upon focusing a laser pulse with the initial phase modulation in the air. The energy of the supercontinuum blue wing is treated as the energy of spectral components $W_{\mathrm{sc}}(z) = \int_{\lambda_{\min}}^{\lambda_{\max}} S(\lambda, z)\mathrm{d}\lambda$, where $S(\lambda, z)$ is varied from $\lambda_{\min} = 500$ nm to $\lambda_{\max} = 700$ nm. One can see that, in the case of a transform-limited pulse ($\tau_{0.5}|_{\delta=0} = 35$ fs, Fig. 6a), the supercontinuum energy is minimal. In the case of a negative phase modulation, despite a decrease in the initial peak power, the energy of the supercontinuum blue wing considerably increases and, for the initial pulse duration $\tau_{0.5}(\delta) = 1200$ fs (Fig. 6b), it becomes more than two orders of magnitude greater

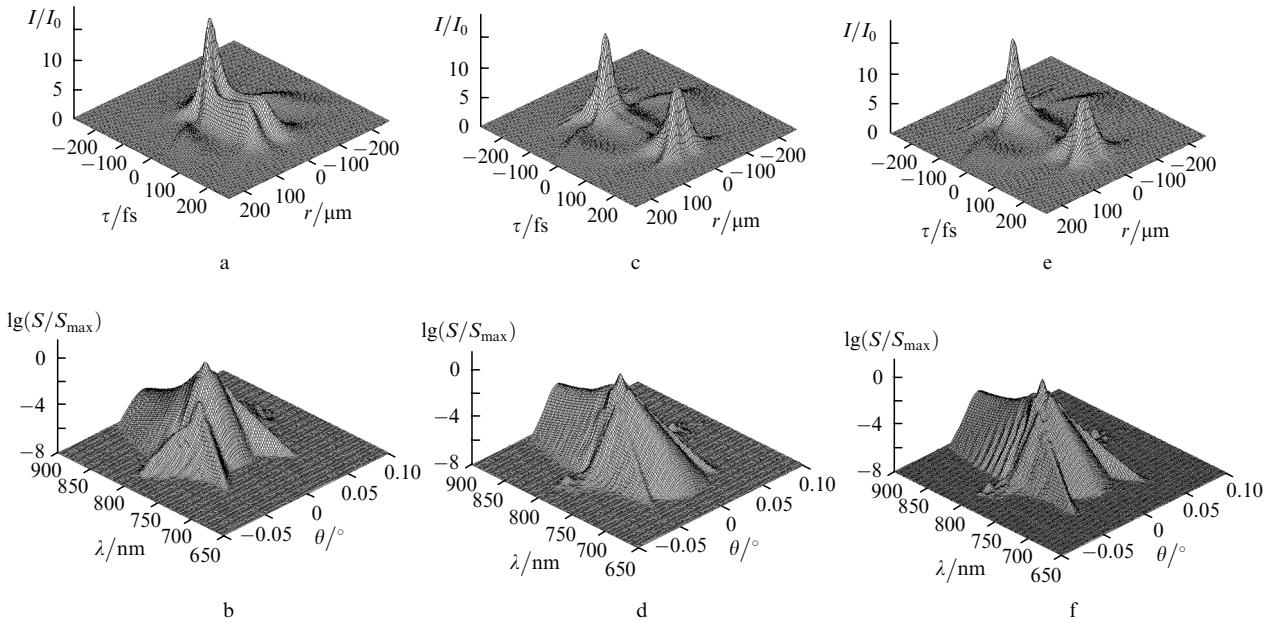

Figure 5. Spatiotemporal intensity distributions (a, c, e) and frequency-angular spectra (b, d, f) of the laser pulse in the air at distances $0.43L_{\mathrm{dif}}$ (a, b) and $0.6L_{\mathrm{dif}}$ (c–f) taking self-steepening into account (a–d) and neglecting it (e, f) for $\tau_{0.5} = 230$ fs, $W_0 = 8$ mJ, and the input beam diameter of 0.28 mm. The intensity $I(r,\tau)$ is normalised to $I_0 = 10^{13}$ W cm^{-2}.

than the energy of the transform-limited pulse. An increase in the efficiency of the supercontinuum generation is explained by the fact that the spatial localisation of energy in the beam cross section due to the geometrical and nonlinear focusing of the beam occurs at the same distance z as the localisation in time caused by the pulse compression. Indeed, a pulse of the initial duration $\tau_{0.5}(\delta) = 1200$ fs undergoes the maximum compression in the air at the distance $z = L_{\rm com} = 0.13L_{\rm dif}$, where $L_{\rm dif} = ka_0^2 = 7000$ m. The nonlinear focusing length $L_{\rm nl}$ for a focused beam can be estimated from the expression [26]

$$\frac{1}{L_{\rm nl}} = \frac{1}{L_{\rm sf}} + \frac{1}{R_{\rm f}}, \tag{8}$$

where $L_{\rm sf}$ is the self-focusing length for a collimated beam. For the initial duration of the laser pulse $\tau_{0.5}(\delta) = 1200$ fs, its peak power is 48 GW. The critical self-focusing power in the air $P_{\rm cr} = 6$ GW, and we obtain, according to Ref. [26], $L_{\rm sf} \simeq 0.19L_{\rm dif}$. According to (8), $L_{\rm nl} = 0.12L_{\rm dif}$, which is close to the compression length $L_{\rm com} = 0.13L_{\rm dif}$.

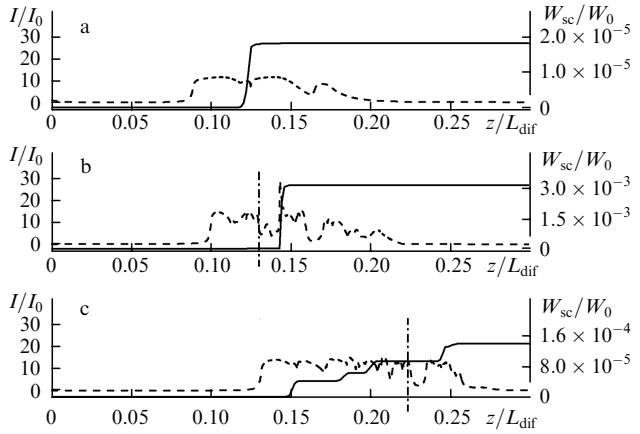

Figure 6. Maximum intensity of the laser pulse with $W_0 = 60$ mJ, $a_0 = 3$ cm for $R_{\rm f} = 0.3L_{\rm dif}$ (dashed curves) and the energy of the supercontinuum blue wing (solid curves) as functions of the distance z in the case of focusing in the air of the transform-limited laser pulse for $\tau_{0.5}|_{\delta=0} = 35$ fs and $L_{\rm com} = 0$ (a) and of pulses with the negative phase modulation for $\tau_{0.5}(\delta) = 1200$ fs, $L_{\rm com} = 0.13L_{\rm dif}$ (b) and $\tau_{0.5}(\delta) = 2000$ fs, $L_{\rm com} = 0.22L_{\rm dif}$ (c). The pulse intensity is normalised to $I_0 = 10^{13}$ W cm^{-2}. The dot-and-dash vertical straight lines indicate the compression length $L_{\rm com}$.

On the contrary, the 35-fs transform-limited pulse, having propagated the distance $z = L_{\rm nl} = 0.02L_{\rm dif}$, spreads due to the material dispersion and its duration increases up to 180 fs, resulting in a decrease in its peak intensity and an increase in the distance between the filament onset and the exit aperture. As a result, the pulse duration achieves 800 fs in the nonlinear focus at the distance $z = 0.09L_{\rm dif}$, the time gradient of the induced phase decreases, and hence, the efficiency of the supercontinuum generation also decreases. For a pulse with the initial duration of 2000 fs, the density of energy in space occurs much faster than the pulse compression because $L_{\rm com} > L_{\rm nl}$, which also leads to a decrease in the supercontinuum energy compared to the energy of the pulse with the initial duration of 1200 fs.

The above estimates can be generalised to pulses with different ratios of lengths of nonlinear focusing $L_{\rm nl}$ and time compression $L_{\rm com}$. Figure 7 shows the diagram of the supercontinuum generation efficiency in the ($L_{\rm nl}$, $L_{\rm com}$) plane obtained in numerical experiments. Different curves correspond to pulses with different initial energies, spectral widths, beam radii, and geometrical focusing lengths. The regions of variations in $L_{\rm nl}$ and $L_{\rm com}$ correspond to some range of the relative energies $W_{\rm sc}/W_0$ of the blue part of the supercontinuum (shown in the figure). The thick straight line divides the regions in which the inequalities $L_{\rm nl} > L_{\rm com}$ and $L_{\rm nl} < L_{\rm com}$ are valid.

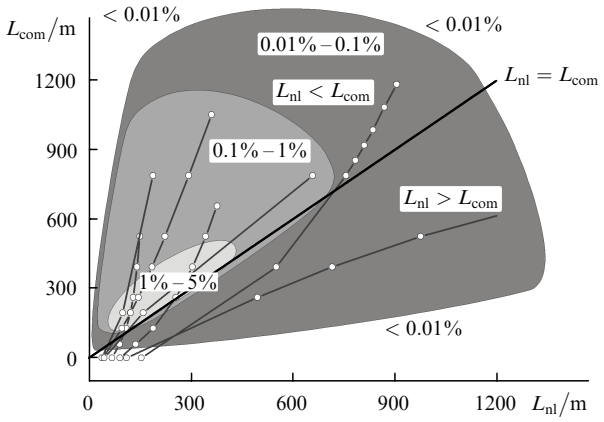

Figure 7. Dependences of the pulse compression length $L_{\rm com}$ on the nonlinear focusing length $L_{\rm nl}$ for different initial phase modulations of the laser pulse. Different curves correspond to laser pulses with different initial parameters. The characteristic supercontinuum generation efficiencies are indicated (in percent) in typical regions of variation of parameters $L_{\rm nl}$ and $L_{\rm com}$.

These data demonstrate that the initial phase modulation of the laser pulse strongly affects the supercontinuum generation efficiency. The supercontinuum has the highest energy (1 % – 5 % of the initial pulse energy) in the region located close to the straight line $L_{\rm nl} = L_{\rm com}$. The supercontinuum generation efficiency decreases away from this straight line, the decrease being greater in the region $L_{\rm nl} > L_{\rm com}$. This is explained by the fact that the time compression of the pulse occurs in this region before the filamentation onset, whereas for $L_{\rm nl} < L_{\rm com}$, due to the filament extension, the maximum time compression of the pulse can occur at the high energy density in the filament formed.

6. Conclusions

We have studied in detail the supercontinuum generation during the propagation of high-power femtosecond laser pulses in continuous transparent media – air and water, at the different initial parameters of laser pulses.

It has been shown that the supercontinuum is generated due to the self-phase spatial and temporal modulation of the laser pulse upon the nonlinear-optical interaction of radiation with the medium in the case of a high spatiotemporal localisation of the field.

We have found in our study that:

(i) The frequency-angular spectrum of the supercontinuum is determined by the spatiotemporal distribution of the nonlinear phase shift in a pulse with a continuous multiring structure caused by the Kerr and plasma nonlinearities, and

wave effects of diffraction and dispersion. The supercontinuum sources are located in the vicinity of edge phase dislocations at the intensity minima of the ring structure. The sources of the low-frequency spectral components are located near rings of a smaller radius and their radiation is directed to the axis, while the sources of the high-frequency components are located near peripheral rings and their radiation is directed from the axis, which is manifested in conical emission.

(ii) The self-steepening makes a significant contribution to the broadening of the pulse spectrum, resulting in an increase in the steepness of the trailing edge of the pulse upon self-focusing and, hence, in an increase in the intensity of high-frequency components in the pulse spectrum.

(iii) The angle of conical emission in the presence of geometrical focusing depends on the geometrical focusing length of the output beam. The divergence angle of conical emission of a focused pulse can be estimated as the sum of the far-field divergence of the beam and the divergence angle of conical emission during the filamentation of a collimated beam.

(iv) The supercontinuum generation efficiency can be increased in media with a normal dispersion by using laser pulses with a negative phase modulation. The 'time' focusing of radiation caused by the dispersion of such pulses in the medium leads to the increase in the energy density in the region of nonlinear interaction. The supercontinuum generation efficiency achieves a maximum when the compression length of the pulse with the initial phase modulation is equal or slightly exceeds the total nonlinear focusing length caused by self-focusing and geometrical focusing.

Acknowledgements. This work was supported by the Russian Foundation for Basic Research (Grant Nos 03-02-16939 and 03-02-06217) and by the European Research Office of the US ARMY (Contract No. 62558-03-M-0029).

References

1. Alfano R. (Ed.) *The Supercontinuum Laser Source* (Berlin: Springer-Verlag, 1989).
2. Kandidov V.P., Kosareva O.G., Golubtsov I.S., Liu W., Becker A., Akozbek N., Bowden C.M., Chin S.L. *Appl. Phys. B*, **77**, 149 (2003).
3. Corkum P.B., Rolland C., Srinavasan-Rao T. *Phys. Rev. Lett.*, **57**, 2268 (1986).
4. Kosareva O.G., Kandidov V.P., Brodeur A., Chien C.Y., Chin S.L. *Opt. Lett.*, **22**, 1332 (1997).
5. Nibbering E.T.J., Curley P.F., Grillon G., Prade B.S., Franco M.A., Salin F., Mysyrowicz A. *Opt. Lett.*, **21**, 62 (1996).
6. Kasparian J., Sauerbrey R., Mondelian D., Niedermeier S., Yu J., Wolf J.-P., Andre Y.-B., Franco M., Prade B., Tzortzakis S., Mysyrowicz A., Rodriguez M., Wille H., Woste L. *Opt. Lett.*, **25**, 1397 (2000).
7. Golubtsov I.S., Kandidov V.P., Kosareva O.G. *Kvanovaya Elektron.*, **33**, 525 (2003) [*Quantum Electron.*, **33**, 525 (2003)].
8. Liu W., Kosareva O., Golubtsov I.S., Iwasaki A., Becker A., Kandidov V.P., Chin S.L. *Appl. Phys. B*, **76**, 215 (2003).
9. Dubietis A., Tamosauskas G., Diomin I., Varanavicius A. *Opt. Lett.*, **28**, 1269 (2003).
10. Xing Q., Yoo K.M., Alfano R.R. *Appl. Opt.*, **32**, 2087 (1993).
11. Yang G., Shen Y.R. *Opt. Lett.*, **9**, 510 (1984).
12. Golub I. *Opt. Lett.*, **15**, 305 (1990).
13. Crenshaw M.E., Cantrell C.D. *Phys. Rev. A*, **39**, 126 (1989).
14. Rae S.C. *Opt. Commun.*, **104**, 330 (1994).
15. Ter-Mikaelian M.L., Torosian G.A., Grigoryan G.G. *Opt. Commun.*, **119**, 56 (1995).
16. Peatross J., Backus S., Zhou J., Murnane M.M., Kapteyn H.C. *J. Opt. Soc. Am. B*, **15**, 186 (1998).
17. Kosareva O.G., Kandidov V.P., Brodeur A., Chin S.L. *Nonlinear Opt. Phys. & Mat.*, **6**, 485 (1997).
18. Golubtsov I.S., Kandidov V.P., Kosareva O.G. *Opt. Atm. Okean.*, **14**, 335 (2001).
19. Chin S.L., Brodeur A., Petit S., Kosareva O.G., Kandidov V.P. *Nonlinear Opt. Phys. & Mat.*, **8**, 121 (1999).
20. Akozbek N., Scalora M., Bowden C.M., Chin S.L. *Opt. Commun.*, **191**, 353 (2001).
21. Ranka J.K., Gaeta A.L. *Opt. Lett.*, **23**, 534 (1998).
22. Brabec T., Krausz F. *Phys. Rev. Lett.*, **78**, 3282 (1997).
23. Bakhtin M.A., Shpolyanskii Yu.A., in *Sovremennye tekhnologii. Trudy molodykh uchenykh* (Modern Technologies: Works of Young Scientists) (St. Petersburg: Izd. ITMO, 2001) p. 19.
24. Mlejnek M., Wright E.M., Moloney J.V. *Opt. Lett.*, **23**, 382 (1998).
25. Baranova N.B., Zel'dovich B.Ya. *Zh. Eksp. Teor. Fiz.*, **80**, 1789 (1981).
26. Marburger J.H. *Prog. Quantum Electron.*, **4**, 35 (1975).